Atmos. Chem. Phys. Discuss., 14, 985–1018, 2014
www.atmos-chem-phys-discuss.net/14/985/2014/
doi:10.5194/acpd-14-985-2014

Atmospheric Chemistry and Physics Discussions

Online measurements of water-soluble organic acids in the gas and aerosol phase from the photooxidation of 1,3,5-trimethylbenzene

A. P. Praplan[1,*], K. Hegyi-Gaeggeler[1], P. Barmet[1], L. Pfaffenberger[1], J. Dommen[1], and U. Baltensperger[1]

[1]Laboratory of Atmospheric Chemistry, Paul Scherrer Institute, Villigen PSI, Switzerland
[*]now at: Division of Atmospheric Sciences, University of Helsinki, Helsinki, Finland

Received: 25 November 2013 – Accepted: 27 December 2013 – Published: 13 January 2014

Correspondence to: J. Dommen (josef.dommen@psi.ch)

Published by Copernicus Publications on behalf of the European Geosciences Union.

Abstract

The formation of organic acids during photooxidation of 1,3,5-trimethylbenzene (TMB) was investigated with an online ion chromatography (IC) instrument coupled to a mass spectrometer (MS) at the Paul Scherrer Institute (PSI) smog chamber. Gas and aerosol phase were both sampled. Molecular formulae were attributed to twelve compounds with the help of high resolution MS data from filter extracts (two compounds in the gas phase only, two in the aerosol phase only and eight in both). Seven of those species could be identified unambiguously (each of them present in gas and aerosol phase): formic acid, acetic acid, glycolic acid, butyric acid, pyruvic acid, lactic acid and methylmaleic acid. The influence of the precursor concentration (TMB: 1200 and 600 ppbv) and of the presence of 2 ppbv of sulphur dioxide (SO_2) on aerosol and gas phase products were further investigated. While the organic acid fraction present in the aerosol phase does not strongly depend on the precursor concentration (6 to 14 %), the presence of SO_2 reduces this amount to less than 3 % for both high and low precursor concentration scenarios. The addition of acetic acid during the experiments indicated that the presence of small acids in the particle phase might not be due to partitioning effects.

1 Introduction

Aromatic compounds are ring-containing volatile organic compounds (VOCs) emitted into the atmosphere by fuel combustion and evaporation, where they are oxidised by hydroxyl radicals ($OH^{\bullet}$) or nitrate radicals ($NO_3^{\bullet}$). They play a major role in urban areas and can represent 13–44 % of the total hydrocarbon mass in the atmosphere (Calvert, 2002; Dommen et al., 2003; Molina et al., 2007; Vega et al., 2011). As a result of their oxidation, products with lower volatility are formed, which contribute to the formation of secondary organic aerosol (SOA).

ACPD
14, 985–1018, 2014

The organic fraction of the atmospheric aerosol, to which SOA contributes, is a complex mixture of many different compounds. Decesari et al. (2000) reported that 20–70 % of these compounds are water soluble organic compounds (WSOC). However, only 10 % of this water soluble organic fraction of the aerosol can typically be chemically identified.

Organic acids represent an important class of atmospheric chemical compounds (Chebbi and Carlier, 1996) and a large fraction of WSOC. Even though they can be directly emitted into the atmosphere by traffic (Kawamura et al., 2000), biogenic emissions (Servant et al., 1991) and biomass burning (Gaeggeler et al., 2008), they also can be produced by ozonolysis of alkenes through electrophilic addition and formation of Criegee intermediates and their subsequent stabilization by peroxyl radicals ($HO_2^\bullet$), by reaction of alkylperoxy radical ($RO_2^\bullet$) with $HO_2^\bullet$ (Madronich et al., 1990), by reaction of $RO_2^\bullet$ with an acyloxy radical as well as by ester rearrangement. Aqueous oxidation in cloud droplets is an important source of organic acids in the atmosphere as well (Altieri et al., 2008; Lim et al., 2005).

Measurement of organic acids is a challenging task. Offline methods are prone to artefacts and are labour-intensive, while online methods providing high time resolution and low detection limits are scarce. Although a proton-transfer-reaction mass spectrometer (PTR-MS) can detect acids, several compounds and/or fragments can have the same m/z, which makes data analysis and interpretation for unit mass resolution data difficult. The ion chromatography (IC) method presented here allows selective collection of organic acids and their separation prior to detection. By using a mass spectrometer (MS) as an additional detector, further separation based on molar mass can be performed on coeluting peaks.

Fisseha et al. (2004) identified 20 different acids formed during 1,3,5-trimethylbenzene (TMB) photooxidation experiments at the Paul Scherrer Institute smog chamber. The main goal of this work is to investigate further organic acids formation and evolution over time during TMB photooxidation under different experimental conditions.

ACPD
14, 985–1018, 2014

2 Experimental

2.1 PSI smog chamber

A detailed description of the smog chamber at the Paul Scherrer Institute (PSI) can be found elsewhere (Paulsen et al., 2005). Experiments are carried out in a 27 m^3 transparent fluoroethylene propylene (FEP) bag placed in a temperature-controlled housing (~ 20 °C). The chamber is first humidified to a relative humidity (RH) of approximately 50 % before injecting nitrogen oxides (NO_x). A known amount of liquid TMB is evaporated in a heated glass sampling bulb (80 °C) and flushed with pure air into the chamber approximately 30 min before the lamps are switched on, to allow homogeneous mixing of all gas phase compounds. To simulate the solar spectrum, four 4 kW xenon-arc lamps are used (light spectrum > 280 nm) and directed parallel to the chamber walls. In selected experiments, supplementary black lights (eighty 100 W tubes, light spectrum between 320 and 400 nm, Cleo Performance) were used to increase the ultraviolet (UV) light intensity. Light is reflected by aluminium plates covering the inside of the housing walls of the chamber and is responsible for hydroxyl radical ($OH^{\bullet}$) formation, by ozone photolysis. For the representative experiments described here (Table 1), the ratio VOC : NO_x was set to 2. For some experiments, approximately 2 ppbv of sulphur dioxide (SO_2) were also injected into the chamber in order to enhance the nucleation rate, to increase the SOA particle number concentration and to reduce vapour wall losses.

The standard instrumentation of the smog chamber consists of ozone (O_3) and NO_x monitors, a condensation particle counter (CPC) with a cut-off of 3 nm and a scanning mobility particle sizer (SMPS) for particles with mobility diameter between 14 and 698 nm. Additionally, a PTR-MS (Ionicon Analytical GmbH, Austria) for the analysis of gas phase compounds and an IC coupled to a MS for the selective analysis of organic acids (Sect. 2.2) were used.

ACPD
14, 985–1018, 2014

2.2 Ion chromatography system

The sampling of the gas and particle phase for the IC system was done with a wet effluent diffusion denuder (WEDD) and an aerosol collector (AC), respectively (Takeuchi et al., 2004, 2005). The WEDD part is connected through a Teflon® inlet to the smog chamber. It consists of two parallel cellulose acetate membranes between which continuous sampling from the smog chamber gas phase occurs. Purified water flows on the other side of the membranes, allowing gases to dissolve. The AC part is connected by a silcosteel® inlet to the smog chamber. An activated charcoal denuder and a WEDD are placed upward the sampling line, to remove the gas phase compounds. Figure 1 shows that after placing a filter on the sampling line, the measured aerosol concentrations return to background level. No breakthrough of the gas phase to the aerosol collector occurs, even with high precursor concentrations. The AC consists of a small chamber, the bottom of which is covered by a filter paper placed on a hydrophilic filter. Water is introduced into this chamber through a capillary having its tip close to the nozzle where the airflow enters. A fine mist is formed, which condenses on the filter where the soluble compounds of the particles are dissolved.

Effluents from both sampling devices pass through concentration columns (TAC-LP1, Dionex) where the (organic and inorganic) anions are retained. Those samples are then eluted alternately to the guard and analytical columns (NG1 and AS11-HC, Dionex) for separation. The eluent consists of a hydroxy anion (OH^-) gradient: 0 min 0.95 mM OH^-, 3 min 0.95 mM OH^-, 18 min 12 mM OH^-, 22 min 60 mM OH^-, 24 min 60 mM OH^-, 24.1 min 0.95 mM OH^- and 29 min 0.95 mM OH^-. After elution, the OH^- are suppressed by an anion self-regenerating suppressor (ASRS 300 2 mm, Dionex). The analytes are detected as deprotonated species by a conductivity detector (CD) first and, after negative electrospray ionisation ((–)ESI), by a quadrupole MS (MSQ, ThermoFinnigan) with unity mass resolution.

The retention time (RT) of the analytes depends on the strength of the ion exchange with the analytical column. Deprotonated organic acids with only one carboxylic func-

ACPD
14, 985–1018, 2014

tional group will elute earlier, followed by acids with two and three carboxylic functional groups at later RTs.

Calibration is performed by direct injection of aqueous multi-compound standards of different concentrations onto the analytical column. Non-linear least squares regression of a power function ($y = ax^b + c$) is used as calibration curve for the MS, in order to take into account the slight curvature of some calibration curves (Fig. 2), as suggested by Kirkup and Mulholland (2004). This is due to the formation of dimers and aggregates with water during ESI, especially at higher concentrations, and possibly varying fragmentation (Grossert et al., 2005) at different concentration levels. Due to the presence of numerous unknown compounds, it is not possible to tune the instrument for each individual substance to prevent the formation of dimers, for example.

If a molecular formula could be assigned to an unknown compound, a surrogate compound with a similar degree of unsaturation (expected similar functionalisation, see Sect. 2.3) and a similar mass was used for calibration.

2.3 High resolution MS

The high resolution Orbitrap-MS instrument of the Functional Genomics Center Zurich is described in details elsewhere (Olsen et al., 2007). The high mass accuracy (2 ppm) allows deduction of the accurate elemental composition of the detected organic acids. From the obtained chemical formula, it is then possible to compute their degree of unsaturation (DU), also known as "double bond equivalent", using Eq. (1), where C, H and N represent the number of carbon, hydrogen and nitrogen atoms, respectively.

$$\mathrm{DU} = (\mathrm{C} + 1) - \frac{(\mathrm{H} - \mathrm{N})}{2} \quad (1)$$

It provides the number of double bonds or rings of a compound and can help for the structure elucidation of an unknown compound: for example, monocarboxylic acids with DU > 1 contain a ring structure or a carbon–carbon double bond if O = 2 (O represents the number of oxygen atoms) or may contain one or more ketone or aldehyde func-

ACPD
14, 985–1018, 2014

tionalities if O > 2. The deductions are similar for the dicarboxylic acids with DU > 2. Furthermore, if O > 2 for monocarboxylic acids with DU = 1 or if O > 4 for dicarboxylic acids with DU = 2, the oxygen atoms that are not in the carboxylic functional groups are most likely present as alcohol functional groups. In this study, N = 0 is assumed as no even m/z was detected and it is unlikely that species with two nitrogen atoms are detected but none with only one N-atom.

For these measurements, SOA particles were collected on filters and extracted with water. The solutions were finally directly injected into the instrument, whose measurements ranged from m/z 50 to 700 amu.

2.4 Partitioning theory

One important feature of the WEDD/AC-IC/MS setup presented is that it is possible to measure almost simultaneously gas phase and aerosol concentrations of the organic acids. Therefore, partitioning coefficients K_p [$m^3\,\mu g^{-1}$] can be determined experimentally by Eq. (2) and estimated theoretically by Eq. (3), using partitioning theory (Pankow, 1994a, b).

$$K_{p,i} = \frac{F_i}{f_m \cdot \mathrm{TSP} \cdot A_i} \quad (2)$$

$$K_{p,i} = \frac{f_m \cdot 760 \cdot R \cdot T}{\mathrm{MW}_m \cdot p_L^0 \cdot \xi \cdot 10^6} \quad (3)$$

TSP [$\mu g\,m^{-3}$] is the total suspended particulate mass and f_m represents its absorbing mass fraction (assumed to be unity for SOA). F_i and A_i [$\mu g\,m^{-3}$] are the measured aerosol and gas phase concentrations of species i, respectively. R is the ideal gas constant ($8.2 \times 10^{-5}\,m^3\,atm\,mol^{-1}\,K^{-1}$), T [K] is the temperature, MW_m is the mean molecular weight of the absorbing material and is assumed here to be $130\,g\,mol^{-1}$. ξ is the activity coefficient of the species in the condensed phase (assumed to be

ACPD
14, 985–1018, 2014

unity) and p_L^0 [Torr] is the saturation vapour pressure. A theoretical range for p_L^0 can be determined with structure-based estimations[1] (Stein and Brown, 1994; Myrdal and Yalkowsky, 1997; Nannoolal et al., 2004; Moller et al., 2008; Nannoolal et al., 2008; Compernolle et al., 2011). The partitioning of organic acids is also influenced by their dissociation in the particle phase which depends on pH ($-\log[H^+]$). Acid dissociation is not considered for K_p values derived from Eq. (3) which is representative for a very acidic aerosol. Thus for less acidic or neutralized aerosols an effective partitioning coefficient ($K_{p,\,eff}$) needs to be calculated using dissociation constants of acids (K_a), determined for aqueous solutions, according to Eq. (4).

$$K_{p,\,eff,\,i} = K_{p,\,i}\left(1 + \frac{K_a}{[H^+]}\right) \quad (4)$$

However, since TMB SOA is only slightly hygroscopic (Duplissy et al., 2011), the fraction of organic material in the particles remains fairly large.

2.5 Chemicals

Water used for this work was delivered by a Milli-Q water purification system and had a resistivity of 18 MΩ cm. TMB was supplied by Fluka (purity: 99.5 %). Gas cylinders were provided by Carbagas: NO 2.8 in N_2 5.0, NO_2 1.8 in synthetic air 5.0 and SO_2 3.8 in N_2 5.0.

3 Results and discussion

3.1 TMB photooxidation

Figure 3 presents the measured mixing ratios of NO, NO_2 and O_3. Ozone photolysis triggers the formation of $OH^\bullet$ radicals, which oxidise TMB. Oxidation products are

[1] http://www.aim.env.uea.ac.uk/aim/ddbst/pcalc_main.php

ACPD
14, 985–1018, 2014

formed and when NO has reached low levels, the formation of O_3 strongly increases. This happens much faster with the stronger black lights. Figure 4b shows the $OH^\bullet$ concentration derived from TMB reacted measured with PTR-MS (Fig. 4a), as TMB does not react with any other oxidant. As expected, the values using black lights are higher: ca. 2.5×10^6 with a peak at 6.5×10^6 at the beginning of the experiment, compared to values between 10^5 and 10^6 for the other experiments. All values are in the lower range of daytime $OH^\bullet$ concentration in the troposphere. The low concentration experiment without SO_2 nor black lights is not displayed as no PTR-MS data is available for this experiment. However, as this experiment was performed at similar RH and with the same lights as the ones with high TMB concentration, the $OH^\bullet$ concentration is expected to be similar.

3.2 SOA formation

Physical aerosol properties from four out of the six experiments are shown in Fig. 5 where low concentration experiments are coloured blue and high concentration experiments red. The lowest panel of Fig. 5 presents the aerosol mass concentration measured by the SMPS assuming a particle density ρ_p of $1.4\,g\,cm^{-3}$ (Alfarra et al., 2006).

Particles sufficiently large to be detected are formed when the NO mixing ratio becomes low in the system, similarly to earlier observations (Ng et al., 2007; Wyche et al., 2009). The SOA particles reached mobility diameters up to ~700 nm during the photooxidation of 1200 ppbv TMB in the absence of SO_2. This is on the edge of the SMPS measurement range for singly charged particles. Therefore, the particle number size distribution was recovered from the raw signal of the doubly charged particles, which appeared at smaller diameters within the measurement range, using a custom-made data inversion routine, which works in a similar way as the standard SMPS data inversion (Hagen and Alofs, 1983). The very narrow size distribution and thus the clear separation between singly and multiple charged particles allowed to use this approach.

ACPD
14, 985–1018, 2014

In the absence of SO_2 (Fig. 5, solid lines), more SOA is produced at higher precursor concentration than with a lower precursor concentration but its formation starts later and the particles formed are bigger. From the CPC data (not shown), particles larger than 3 nm can be observed after approximately 3.2 h after lights on during the experiments with 1200 ppbv TMB while in the case with 600 ppbv nucleation occurs already after 2 h of photooxidation.

The presence of SO_2 increases the nucleation rate as described in Metzger et al. (2010): it is possible to observe particles in the CPC (> 3 nm) already after 1 h of photooxidation (1200 ppbv TMB). The slightly higher final aerosol mass concentration produced in the presence of SO_2 during the high concentration experiments is probably explained by the earlier particle formation, resulting in lower vapour wall losses of low-volatility oxidation products.

Black lights increase the nucleation rate the most, due to the higher $OH^{\bullet}$ exposure and concentration and faster oxidation of the gaseous compounds. With black lights switched on, 12 min of photooxidation are sufficient to detect particles with the CPC in the presence of SO_2. The maximum aerosol mass produced increases by roughly a factor of 2 because of the higher amount of TMB reacted, but also due to dramatical reduction of the vapour wall losses in the early nucleation stage.

3.3 Identified organic acids

Table 2 gives an overview of the organic acids detected during TMB photooxidation. At least one chromatographic peak was identified on twenty-five masses and of those, a chemical formula could be attributed to twelve species with the help of the high resolution MS data. Chemical formulas containing only one oxygen atom were not considered, as carboxylic acids contain at least two oxygen atoms. Seven compounds could be unambiguously identified: formic acid, acetic acid, glycolic acid, butanoic acid, pyruvic acid, lactic acid and methylmaleic acid. Fisseha et al. (2004) did not identify glycolic acid and butanoic acid, but reported detection of oxalic acid, malonic acid, succinic acid, malic acid and citric acid, which were not detected in the present work. The only

ACPD
14, 985–1018, 2014

unknown compounds detected in both studies are the ones with nominal mass 178, 190 and 234.

Sato et al. (2012) could also identify pyruvic acid as well as other organic acids with liquid chromatography coupled to a time-of-flight MS. They found several peaks for all (deprotonated) masses: 127 ($C_6H_7O_3^-$), 161 ($C_6H_9O_5^-$), 215 ($C_9H_{11}O_6^-$) and 233 ($C_9H_{13}O_7^-$) as well as single peaks of the (deprotonated) masses 189 ($C_6H_7O_3^-$) and 217 ($C_9H_{13}O_6^-$), each corresponding to an identified peak in this study. While several possible formulae are reported in Table 2 for these compounds, as it was not possible to unambiguously identify which peaks in the high resolution spectra corresponded to the unity mass observed with IC/MS, Sato et al. (2012) reported unique chemical composition for each mass. They also reported other masses, which were not found in this work, either because they are not organic acids (even though a structure with a carboxylic acid functionality was proposed), or because the sensitivity of our method was not sufficient to detect them.

The Master Chemical Mechanism (MCM, Jenkin et al., 2003; Saunders et al., 2003) contains a degradation scheme for TMB of which Table 3 presents the expected organic acids. Only acetic acid and pyruvic acid could be identified in our experiments. Also acids with nominal mass 128, 144 and 160 were detected, but it was not possible to assign the species proposed by MCM to IC peaks, mainly because more than one peak were found for each of these unit masses and their structure could not be determined. Formation mechanisms for the other identified organic acids is not discussed here, as they are mainly low molar mass compounds and can originate from various oxidation pathways as for acetic acid and pyruvic acid. In addition, the mechanism of later generation products is not well known (Metzger et al., 2008).

It is interesting to note that there is a large variety of compounds with a molar mass higher than TMB (molar mass: 120.19 g mol^{-1}) itself (functionalisation, oligomerisation) while the compounds with smaller molar mass (fragmentation) are less in number but seem to contribute more to the aerosol mass. However, a quantitative comparison between functionalisation/oligomerisation and fragmentation is difficult to address, as the

ACPD
14, 985–1018, 2014

contribution of many compounds cannot be quantified properly, due to a lack of standards for calibration.

Two of the compounds for which a chemical formula could be attributed have a DU equal to 4 (DU of TMB), while ten have a lower DU. This indicates that fragmentation and double bond opening reactions happen on top of the functionalisation with one or two carboxylic groups (1 DU for each group).

Figures 6 and 7 show the concentration profiles in the gas and the aerosol phase, respectively, for the main measured species: formic acid, acetic acid, glycolic acid, butanoic acid, pyruvic acid, lactic acid, methylmaleic acid and an unknown dicarboxylic acid with molar mass 234 $g\,mol^{-1}$ (M234). Some of these species were close to the detection limit of the method and therefore gaps can be observed in the plots. Methylmaleic acid is a dicarboxylic acid and is not expected with such high concentrations in the gas phase (without being detected accordingly in the aerosol phase at the same time). Most probably it is formed from the expected methylmaleic anhydride in the sampling device. Note that other detected species could also be formed by similar artefacts from other compounds.

The production of glycolic acid in both gas and aerosol phase remains small and does not seem to depend on the precursor concentration. Butyric acid, pyruvic acid and methylmaleic acid gas phase concentrations show a precursor concentration dependence, confirming that they are products of TMB oxidation. For lactic acid, a marked difference is seen comparing the 1200 ppbv TMB experiments. The presence of SO_2 decreases its concentration by roughly a factor 3. Recent studies show that SO_2 reacts much faster with Criegee radicals than previously reported (Welz et al., 2012; Boy et al., 2012; Mauldin III et al., 2012). The differences in the experiments with and without SO_2 could be explained by reaction of the precursor Criegee radical with that species, hindering the formation of lactic acid.

In the aerosol phase the measured concentrations are mostly lower than 1 $\mu g\,m^{-3}$, except for M234. The presence of SO_2 decreases the aerosol concentration for this species, as well as for lactic acid and butanoic acid. Due to the different aerosol mass

ACPD
14, 985–1018, 2014

concentrations produced, acid fractions were computed by dividing the particle bound acid concentration with the aerosol mass concentration measured by SMPS. Figure 8c and d shows a drop of the acid fraction of the main acids below 3 % after 5 h of photooxidation if SO_2 is present, while independently of the precursor concentration, its lower limit lies between 6 and 14 % in the absence of SO_2 (Fig. 8a and c). This is expected, because less partitioning of the organic acids occurs, due to the more acidic aerosol in the presence of H_2SO_4 formed from SO_2 oxidation.

The compound M234 merits particular attention. It is the most abundant organic acid of the aerosol phase. It could be detected in small amounts in the gas phase and is potentially important for the SOA formation. Sato et al. (2012) report three compounds with this mass and the chemical formula ($C_9H_{14}O_7$), while we could identify only one peak with this mass in the range of dicarboxylic acids. Very likely, the two other compounds are hydroxycarbonyl compounds without carboxylic acid functional group, so that the isomer structure proposed by Sato et al. (2012) does not correspond to any of the compounds with nominal mass 234 (one dicarboxylic acid and two hydroxycarbonyl compounds).

Also, the unknown compound at m/z 85 has a longer RT than methacrylic acid, 3-butenoic acid and *trans*-2-butenoic acid. *cis*-2-Butenoic acid was not tested due to the lack of available standard so that it cannot be ruled out. The longer RT could be explained by its somewhat compacter shape allowing it to remain longer on the analytical column.

Due to the remaining uncertainties, more work is needed to identify the chemical structure of the numerous compounds that are formed during photooxidation of TMB. A combination of different analytical techniques like gas or liquid chromatography with high-resolution mass spectrometry would be necessary.

3.4 Partitioning coefficients, K_p

Figure 9 depicts the time-dependent K_p values for the previously discussed species. Due to the alternating gas phase and aerosol measurements, linear interpolation or

ACPD
14, 985–1018, 2014

extrapolation was performed to estimate the corresponding aerosol or gas phase concentration for a given time. Nevertheless, due to some measurements very close to the detection limit, especially in the aerosol phase, some points could not be estimated. In most cases, the experimental K_p values for the different conditions are more or less stable during the experiments. Only for glycolic acid and methylmaleic acid, a decreasing trend is observed in the earlier stages of the experiment. This is very likely due to measurements close to the detection limits in the aerosol phase for these species, so that the decrease mainly reflects the TSP increase in this case.

Aerosol mass spectrometer measurements (not shown) indicate that nitric acid is the main inorganic species present in the aerosol phase and that it is not neutralised by ammonia, whose concentration is much lower. Ammonia was not added deliberately but is an impurity trace gas in the chamber, which has also been determined previously for similar conditions (Kalberer et al., 2004). Therefore, the following discussion holds for these acidic aerosol conditions (assuming pH < 3). The presence of H_2SO_4 from SO_2 oxidation will decrease the pH of the aerosol. However, there is no clear influence of SO_2 in the experiments with 1200 ppbv of TMB except for glycolic acid. In the presence of SO_2, less glycolic acid remains in the gas phase. This is the opposite behaviour of what would be expected. For the experiments with 600 ppbv of TMB, K_p values are somewhat lower in the presence of SO_2, as expected for a more acidic aerosol.

Overall, the experimental values obtained are much higher than the theoretically estimated values, derived from different estimated values for p_L^0. The upper limit of the theoretical value takes into consideration the dissociation of acids in the aerosol phase, assuming a pH value of 4. Weak acids like acetic and butanoic acid are not much affected by this assumption, while the theoretical K_p range for stronger acids like formic, glycolic and lactic acid is increased due to the larger deprotonated acid fraction present in the aerosol at this pH value. Nevertheless, the discrepancy between the estimated K_p values and the experimentally determined ones remains large, supporting the hypothesis of a measurement artefact or a source of carboxylate ions in the aerosol phase.

ACPD
14, 985–1018, 2014

Interestingly, the K_p values of methylmaleic acid fall in the range of the theoretical values for methylmaleic anhydride (light grey shaded area). This confirms that no methylmaleic acid (or a negligible amount) is formed in the chamber. It would also indicate that partitioning is not further driven by hydrolysis of the anhydride in the aerosol.

Nevertheless, Healy et al. (2008) found similar results for a wide range of dicarbonyl products, including glyoxal and methylglyoxal. The interpretation given was that reactive uptake as well as oligomerisation reaction in the particle phase take place, shifting the partitioning to the aerosol, which may also happen with organic acids. Then, because during sampling in water, the oligomers can reverse to their monomeric form, the aerosol concentration is found to be higher than expected.

During the experiment of 10 July 2009, a very large amount of acetic acid ($\sim 18\,\mathrm{mg\,m^{-3}}$) was injected into the chamber after roughly 6 hours of photooxidation. Figure 10 shows that this results in almost no increase of the aerosol phase acetic acid concentration, while according to Henry's law (assuming that the aerosol would take up acetic acid as water would), concentrations between 170 and 2100 $\mathrm{ng\,m^{-3}}$ would be expected. This means that for the observed aerosol concentrations of acetic acid, the corresponding gas phase concentration should be much higher than detected. This is another strong indication that the acetic acid (and probably the other volatile organic acids) detected in the particle phase are not due to (enhanced) partitioning. We assume that their occurrence is the result of the hydrolysis of ester functionalities during sampling or in the aerosol phase.

4 Summary and conclusions

Despite the complexity of the chemical composition of photooxidation products from TMB, we were able to selectively separate and detect several organic acids from both gas and aerosol phases with IC/MS from which seven could be identified unambiguously. A chemical formula could be attributed to five more compounds.

ACPD
14, 985–1018, 2014

Some of the detected compounds were possibly produced during sampling, like methylmaleic acid, by anhydride hydrolysis or other aqueous reactions, for example. However, many of those compounds are present in low concentration and by focusing on the main detected compounds a general picture of the fate of organic acids in TMB photooxidation experiments could be drawn. Overall, their fraction represents less than 3 % of SOA after 5 h of photooxidation in the presence of SO_2, while in its absence, they represent between 6 and 14 % of the SOA mass, independently of the precursor concentration. This is in line with the expectation that organic acids will dissociate less in an acidic aerosol particle and therefore the partitioning to the aerosol phase is lower.

However, higher partitioning coefficients than predicted by theory were found. As it is not possible to link clearly aerosol acidity with an enhanced partitioning into the aerosol phase, this is a strong indication that the method used here may have been influenced by hydrolysis, giving an indication that ester oligomers may be present in the aerosol phase and are hydrolysed during sampling with water. Even an injection of a very large amount of acetic acid did not increase significantly the amount of acetic acid detected in the aerosol phase. This is a strong indication that it arises likely from hydrolysis of ester functionalities during sampling. For this reason, measurements of K_p need to be considered with care.

Acknowledgements. The Functional Genomics Center Zurich and Bertran Gerrits are thanked for the opportunity to perform measurements at the Orbitrap XL, René Richter for his help in building the WEDD/AC, Martin Gysel for his support on the SMPS data analysis and Alexander Wokaun for helpful discussions. This work was supported by the Swiss National Science Foundation as well as the EU FP7 project EUROCHAMP-2.

References

Alfarra, M. R., Paulsen, D., Gysel, M., Garforth, A. A., Dommen, J., Prévôt, A. S. H., Worsnop, D. R., Baltensperger, U., and Coe, H.: A mass spectrometric study of secondary organic aerosols formed from the photooxidation of anthropogenic and biogenic precursors

ACPD
14, 985–1018, 2014

in a reaction chamber, Atmos. Chem. Phys., 6, 5279–5293, doi:10.5194/acp-6-5279-2006, 2006. 993
Altieri, K., Seitzinger, S., Carlton, A., Turpin, B., Klein, G., and Marshall, A.: Oligomers formed through in-cloud methylglyoxal reactions: chemical composition, properties, and mechanisms investigated by ultra-high resolution FT-ICR mass spectrometry, Atmos. Environ., 42, 1476–1490, doi:10.1016/j.atmosenv.2007.11.015, 2008. 987
Boy, M., Mogensen, D., Smolander, S., Zhou, L., Nieminen, T., Paasonen, P., Plass-Dülmer, C., Sipilä, M., Petäjä, T., Mauldin, L., Berresheim, H., and Kulmala, M.: Oxidation of SO_2 by stabilized Criegee intermediate (sCI) radicals as a crucial source for atmospheric sulfuric acid concentrations, Atmos. Chem. Phys., 13, 3865–3879, doi:10.5194/acp-13-3865-2013, 2013. 996
Calvert, J.: The Mechanisms of Atmospheric Oxidation of Aromatic Hydrocarbons, Oxford University Press, New York, USA, 2002. 986
Chebbi, A. and Carlier, P.: Carboxylic acids in the troposphere, occurrence, sources, and sinks: a review, Atmos. Environ., 30, 4233–4249, doi:10.1016/1352-2310(96)00102-1, 1996. 987
Compernolle, S., Ceulemans, K., and Müller, J.-F.: EVAPORATION: a new vapour pressure estimation methodfor organic molecules including non-additivity and intramolecular interactions, Atmos. Chem. Phys., 11, 9431–9450, doi:10.5194/acp-11-9431-2011, 2011. 992
Decesari, S., Facchini, M. C., Fuzzi, S., and Tagliavini, E.: Characterization of water-soluble organic compounds in atmospheric aerosol: a new approach, J. Geophys. Res., 105, 1481–1489, doi:10.1029/1999JD900950, 2000. 987
Dommen, J., Prevot, A., Baertsch-Ritter, N., Maffeis, G., Longoni, M., Grüebler, F., and Thielmann, A.: High-resolution emission inventory of the Lombardy region: development and comparison with measurements, Atmos. Environ., 37, 4149–4161, doi:10.1016/S1352-2310(03)00507-7, 2003. 986
Duplissy, J., DeCarlo, P. F., Dommen, J., Alfarra, M. R., Metzger, A., Barmpadimos, I., Prevot, A. S. H., Weingartner, E., Tritscher, T., Gysel, M., Aiken, A. C., Jimenez, J. L., Canagaratna, M. R., Worsnop, D. R., Collins, D. R., Tomlinson, J., and Baltensperger, U.: Relating hygroscopicity and composition of organic aerosol particulate matter, Atmos. Chem. Phys., 11, 1155–1165, doi:10.5194/acp-11-1155-2011, 2011. 992
Fisseha, R., Dommen, J., Sax, M., Paulsen, D., Kalberer, M., Maurer, R., Höfler, F., Weingartner, E., and Baltensperger, U.: Identification of organic acids in secondary organic aerosol

ACPD
14, 985–1018, 2014

and the corresponding gas phase from chamber experiments, Anal. Chem., 76, 6535–6540, doi:10.1021/ac048975f, 2004. 987, 994

Gaeggeler, K., Prévôt, A. S., Dommen, J., Legreid, G., Reimann, S., and Baltensperger, U.: Residential wood burning in an Alpine valley as a source for oxygenated volatile organic compounds, hydrocarbons and organic acids, Atmos. Environ., 42, 8278–8287, doi:10.1016/j.atmosenv.2008.07.038, 2008. 987

Grossert, J. S., Fancy, P. D., and White, R. L.: Fragmentation pathways of negative ions produced by electrospray ionization of acyclic dicarboxylic acids and derivatives, Can. J. Chem., 83, 1878–1890, doi:10.1139/v05-214, 2005. 990

Hagen, D. E. and Alofs, D. J.: Linear inversion method to obtain aerosol size distributions from measurements with a differential mobility analyzer, Aerosol Sci. Tech., 2, 465–475, 1983. 993

Healy, R. M., Wenger, J. C., Metzger, A., Duplissy, J., Kalberer, M., and Dommen, J.: Gas/particle partitioning of carbonyls in the photooxidation of isoprene and 1,3,5-trimethylbenzene, Atmos. Chem. Phys., 8, 3215–3230, doi:10.5194/acp-8-3215-2008, 2008. 999

Jenkin, M. E., Saunders, S. M., Wagner, V., and Pilling, M. J.: Protocol for the development of the Master Chemical Mechanism, MCM v3 (Part B): tropospheric degradation of aromatic volatile organic compounds, Atmos. Chem. Phys., 3, 181–193, doi:10.5194/acp-3-181-2003, 2003. 995

Kalberer, M., Paulsen, D., Sax, M., Steinbacher, M., Dommen, J., Prevot, A. S. H., Fisseha, R., Weingartner, E., Frankevich, V., Zenobi, R., and Baltensperger, U.: Identification of polymers as major components of atmospheric organic aerosols, Science, 303, 1659–1662, doi:10.1126/science.1092185, 2004. 998

Kawamura, K., Steinberg, S., and Kaplan, I. R.: Homologous series of C1–C10 monocarboxylic acids and C1–C6 carbonyls in Los Angeles air and motor vehicle exhausts, Atmos. Environ., 34, 4175–4191, doi:10.1016/S1352-2310(00)00212-0, 2000. 987

Kirkup, L. and Mulholland, M.: Comparison of linear and non-linear equations for univariate calibration, J. Chromatogr. A, 1029, 1–11, doi:10.1016/j.chroma.2003.12.013, 2004. 990

Lim, H.-J., Carlton, A. G., and Turpin, B. J.: Isoprene forms secondary organic aerosol through cloud processing: model simulations, Environ. Sci. Technol., 39, 4441–4446, doi:10.1021/es048039h, 2005. 987

ACPD
14, 985–1018, 2014

Madronich, S., Chatfield, R. B., Calvert, J. G., Moortgat, G. K., Veyret, B., and Lesclaux, R.: A photochemical origin of acetic acid in the troposphere, Geophys. Res. Lett., 17, 2361–2364, doi:10.1029/GL017i013p02361, 1990. 987

Mauldin III, R. L., Berndt, T., Sipilä, M., Paasonen, P., Petäjä, T., Kim, S., Kurtén, T., Stratmann, F., Kerminen, V.-M., and Kulmala, M.: A new atmospherically relevant oxidant of sulphur dioxide, Nature, 488, 193–196, doi:10.1038/nature11278, 2012. 996

Metzger, A., Dommen, J., Gaeggeler, K., Duplissy, J., Prevot, A. S. H., Kleffmann, J., Elshorbany, Y., Wisthaler, A., and Baltensperger, U.: Evaluation of 1,3,5 trimethylbenzene degradation in the detailed tropospheric chemistry mechanism, MCMv3.1, using environmental chamber data, Atmos. Chem. Phys., 8, 6453–6468, doi:10.5194/acp-8-6453-2008, 2008. 995

Metzger, A., Verheggen, B., Dommen, J., Duplissy, J., Prévôt, A. S. H., Weingartner, E., Riipinen, I., Kulmala, M., Spracklen, D. V., Carslaw, K. S., and Baltensperger, U.: Evidence for the role of organics in aerosol particle formation under atmospheric conditions, P. Natl. Acad. Sci. USA, 107, 6646–6651, doi:10.1073/pnas.0911330107, 2010. 994

Molina, L. T., Kolb, C. E., de Foy, B., Lamb, B. K., Brune, W. H., Jimenez, J. L., Ramos-Villegas, R., Sarmiento, J., Paramo-Figueroa, V. H., Cardenas, B., Gutierrez-Avedoy, V., and Molina, M. J.: Air quality in North America's most populous city – overview of the MCMA-2003 campaign, Atmos. Chem. Phys., 7, 2447–2473, doi:10.5194/acp-7-2447-2007, 2007. 986

Moller, B., Rarey, J., and Ramjugernath, D.: Estimation of the vapour pressure of non-electrolyte organic compounds via group contributions and group interactions, J. Mol. Liq., 143, 52–63, doi:10.1016/j.molliq.2008.04.020, 2008. 992

Myrdal, P. B. and Yalkowsky, S. H.: Estimating pure component vapor pressures of complex organic molecules, Ind. Eng. Chem. Res., 36, 2494–2499, doi:10.1021/ie950242l, 1997. 992

Nannoolal, Y., Rarey, J., Ramjugernath, D., and Cordes, W.: Estimation of pure component properties: Part 1. Estimation of the normal boiling point of non-electrolyte organic compounds via group contributions and group interactions, Fluid Phase Equilibr., 226, 45–63, doi:10.1016/j.fluid.2004.09.001, 2004. 992

Nannoolal, Y., Rarey, J., and Ramjugernath, D.: Estimation of pure component properties: Part 3. Estimation of the vapor pressure of non-electrolyte organic compounds via group contributions and group interactions, Fluid Phase Equilibr., 269, 117–133, doi:10.1016/j.fluid.2008.04.020, 2008. 992

ACPD
14, 985–1018, 2014

Ng, N. L., Kroll, J. H., Chan, A. W. H., Chhabra, P. S., Flagan, R. C., and Seinfeld, J. H.: Secondary organic aerosol formation from *m*-xylene, toluene, and benzene, Atmos. Chem. Phys., 7, 3909–3922, doi:10.5194/acp-7-3909-2007, 2007. 993

Olsen, J. V., Macek, B., Lange, O., Makarov, A., Horning, S., and Mann, M.: Higher-energy C-trap dissociation for peptide modification analysis, Nat. Methods, 4, 709–712, doi:10.1038/nmeth1060, 2007. 990

Pankow, J. F.: An absorption model of the gas/aerosol partitioning involved in the formation of secondary organic aerosol, Atmos. Environ., 28, 189–193, doi:10.1016/1352-2310(94)90094-9, 1994a. 991

Pankow, J. F.: An absorption model of gas/particle partitioning of organic compounds in the atmosphere, Atmos. Environ., 28, 185–188, doi:10.1016/1352-2310(94)90093-0, 1994b. 991

Paulsen, D., Dommen, J., Kalberer, M., Prévôt, A. S. H., Richter, R., Sax, M., Steinbacher, M., Weingartner, E., and Baltensperger, U.: Secondary organic aerosol formation by irradiation of 1,3,5-trimethylbenzene–NO_x–H_2O in a new reaction chamber for atmospheric chemistry and physics, Environ. Sci. Technol., 39, 2668–2678, doi:10.1021/es0489137, 2005. 988

Sato, K., Takami, A., Kato, Y., Seta, T., Fujitani, Y., Hikida, T., Shimono, A., and Imamura, T.: AMS and LC/MS analyses of SOA from the photooxidation of benzene and 1,3,5-trimethylbenzene in the presence of NO_x: effects of chemical structure on SOA aging, Atmos. Chem. Phys., 12, 4667–4682, doi:10.5194/acp-12-4667-2012, 2012. 995, 997

Saunders, S. M., Jenkin, M. E., Derwent, R. G., and Pilling, M. J.: Protocol for the development of the Master Chemical Mechanism, MCM v3 (Part A): tropospheric degradation of non-aromatic volatile organic compounds, Atmos. Chem. Phys., 3, 161–180, doi:10.5194/acp-3-161-2003, 2003. 995

Servant, J., Kouadio, G., Cros, B., and Delmas, R.: Carboxylic monoacids in the air of Mayombe forest (Congo): role of the forest as a source or sink, J. Atmos. Chem., 12, 367–380, doi:10.1007/BF00114774, 1991. 987

Stein, S. E. and Brown, R. L.: Estimation of normal boiling points from group contributions, J. Chem. Inf. Comp. Sci., 34, 581–587, doi:10.1021/ci00019a016, 1994. 992

Takeuchi, M., Li, J., Morris, K. J., and Dasgupta, P. K.: Membrane-based parallel plate denuder for the collection and removal of soluble atmospheric gases, Anal. Chem., 76, 1204–1210, doi:10.1021/ac0348423, 2004. 989

ACPD
14, 985–1018, 2014

Takeuchi, M., Ullah, S. M. R., Dasgupta, P. K., Collins, D. R., and Williams, A.: Continuous collection of soluble atmospheric particles with a wetted hydrophilic filter, Anal. Chem., 77, 8031–8040, doi:10.1021/ac051539o, 2005. 989

Vega, E., Sánchez-Reyna, G., Mora-Perdomo, V., Iglesias, G. S., Arriaga, J. L., Limón-Sánchez, T., Escalona-Segura, S., and Gonzalez-Avalos, E.: Air quality assessment in a highly industrialized area of Mexico: concentrations and sources of volatile organic compounds, Fuel, 90, 3509–3520, doi:10.1016/j.fuel.2011.03.050, 2011. 986

Welz, O., Savee, J. D., Osborn, D. L., Vasu, S. S., Percival, C. J., Shallcross, D. E., and Taatjes, C. A.: Direct kinetic measurements of Criegee intermediate (CH_2OO) formed by reaction of CH_2I with O_2, Science, 335, 204–207, doi:10.1126/science.1213229, 2012. 996

Wyche, K. P., Monks, P. S., Ellis, A. M., Cordell, R. L., Parker, A. E., Whyte, C., Metzger, A., Dommen, J., Duplissy, J., Prevot, A. S. H., Baltensperger, U., Rickard, A. R., and Wulfert, F.: Gas phase precursors to anthropogenic secondary organic aerosol: detailed observations of 1,3,5-trimethylbenzene photooxidation, Atmos. Chem. Phys., 9, 635–665, doi:10.5194/acp-9-635-2009, 2009. 993

ACPD
14, 985–1018, 2014

Table 1. Description of the presented representative 1,3,5-trimethylbenzene (TMB) photooxidation experiments.

Date	Nominal concentrations [ppbv]				RH	Comments
	TMB	NO	NO_2	SO_2		
10 Jul 2009	1200	300	300	–	~ 50 %	injection of acetic acid (500 µL) after approximately 6 h of photooxidation
27 Jul 2009	600	150	150	–	~ 50 %	injection of acetic and formic acids (0.4 µL each) after approximately 5.3 h of photooxidation
10 Dec 2010	1200	300	300	–	~ 50 %	
11 Apr 2011	1200	300	300	2	~ 50 %	
13 Apr 2011	600	150	150	2	~ 50 %	with black lights

ACPD
14, 985–1018, 2014

Table 2. Organic acids detected with WEDD/AC-IC/MS during 1,3,5-trimethylbenzene (TMB) photooxidation.

Trivial name (IUPAC name)	Chemical formula	DU	Molar mass [g mol^{-1}]	Type	RT [min] WEDD	RT [min] AC	m/z
Formic acid (Methanoic acid)	CH_2O_2	1	46.03	Mono	11.4–13.3	11.6–13.4	45
Acetic acid (Ethanoic acid)	$C_2H_4O_2$	1	60.05	Mono	10.5–12.5	9.5–12.7	59, 41
Glycolic acid (Hydroxyethanoic acid)	$C_2H_4O_3$	1	76.05	Mono	10.7–12.6	10.5–12.8	75
Unknown 86	?	?	?	?	15.1–16.4	n. d.[b]	85
Butyric acid (Butanoic acid)	$C_4H_8O_2$	1	88.11	Mono	11.3–13.1	11.6–12.6	87
Pyruvic acid (2-Oxopropanoic acid)	$C_3H_4O_3$	2	88.06	Mono	11.9–13.9	12.5–14.1	87, 105
Lactic acid and hydracrylic acid? (Hydroxypropanoic acid)	$C_3H_6O_3$	1	90.08	Mono	10.0–12.1	10.9–12.4	89, 43
Unknown 116	$C_4H_4O_4$	3	116.07	Di ?	16.5–18.5	16.5–18.4	115
Unknowns 128	several compounds with formula $C_5H_4O_4$, $C_6H_8O_3$ or $C_7H_{11}O_2$						127, 83, 101
Methylmaleic/Methylfumaric? acid ((Z/E?)-2-Methylbutenedioic acid)	$C_5H_6O_4$	3	130.10	Di	23.8–25.1	23.4–25.2	129, 85, 259
Unknown 144	several compounds with formula $C_6H_8O_4$						143, 99
Unknowns 148	several compounds with formula $C_5H_8O_5$ or $C_4H_3O_6$						147
Unknown 156a	$C_7H_8O_4$	4	156.14	Di	17.6–18.9	n. d.	155, 111, 83
Unknown 156b	$C_7H_8O_4$	4	156.14	Di	18.4–19.7	n. d.	155, 137
Unknown 160	$C_6H_8O_5$ or $C_7H_{12}O_4$	?	?	Mono	10.6–12.8	11.1–12.6	159
Unknown 162a	$C_6H_{10}O_5$ or $C_5H_6O_6$	?	?	Mono	11.9–12.2	11.0–12.4	161, 143
Unknown 162b	$C_6H_{10}O_5$ or $C_5H_6O_6$	?	?	Di	21.0–22.7	n. d.	161
Unknown 164	$C_5H_8O_6$	2	164.11	Di	n. d.	22.5–24.2	163
Unknowns 178	several compounds with formula $C_6H_{10}O_6$						177
Unknown 190	$C_7H_9O_6$ or $C_8H_{14}O_5$	?	?	Di	n. d.	20.2–21.6	189, 171, 145
Unknown 208	several compounds with formula $C_7H_{12}O_7$						207, 189
Unknowns 216	several compounds with formula $C_8H_8O_7$ or $C_9H_{12}O_6$ or $C_{10}H_{15}O_5$						215, 153, 113
Unknowns 218	several compounds with formula $C_8H_{10}O_7$ or $C_9H_{14}O_6$						217, 155
Unknown 234[c]	$C_9H_{14}O_7$ or $C_8H_{10}O_8$	?	?	Di	18.6–19.1	18.7–20.1	233, 117, 115, 73
Unknown 250	$C_9H_{14}O_8$	3	250.20	Di	n. d.	20.5–21.6	249, 231

[a] butanoic acid as surrogate,
[b] not detected,
[c] methylmaleic acid as surrogate.

ACPD
14, 985–1018, 2014

Table 3. Expected organic acids and related species from the Master Chemical Mechanism (MCM) model for the oxidation of 1,3,5-trimethylbenzene (TMB).

MCM name	IUPAC name (Trivial name)	Formula	Molar mass
CH3CO2H	Ethanoic acid (Acetic acid)	$C_2H_4O_2$	60.05
HCOCO2H	Oxoethanoic acid (Glyoxylic acid)	$C_2H_2O_3$	74.04
CH3COCO2H	Oxopropanoic acid (Pyruvic acid)	$C_3H_4O_3$	88.06
C5CODBCO2H	2-Methyl-4-oxo-pent-2-enoic acid	$C_6H_8O_3$	128.13
EPXMKTCO2H	3-Acetyl-2-methyloxirane-2-carboxylic acid	$C_6H_8O_4$	144.13
C23O3MCO2H	2-((2-Oxopropanoyl)oxy)propanoic acid	$C_6H_8O_5$	160.12
TMBCO2H	3,5-Dimethylbenzoic acid	$C_9H_{10}O_2$	150.17
TM135MUO2H	(Z)-2-Methyl-3-(4-oxopent-2-en-2-yl)oxirane-2-carboxylic acid	$C_9H_{12}O_4$	184.19
MMALANHY*	3-Methylfuran-2,5-dione (Methylmaleic anhydride)	$C_5H_4O_3$	112.08

* detected as methylmaleic acid.

ACPD
14, 985–1018, 2014

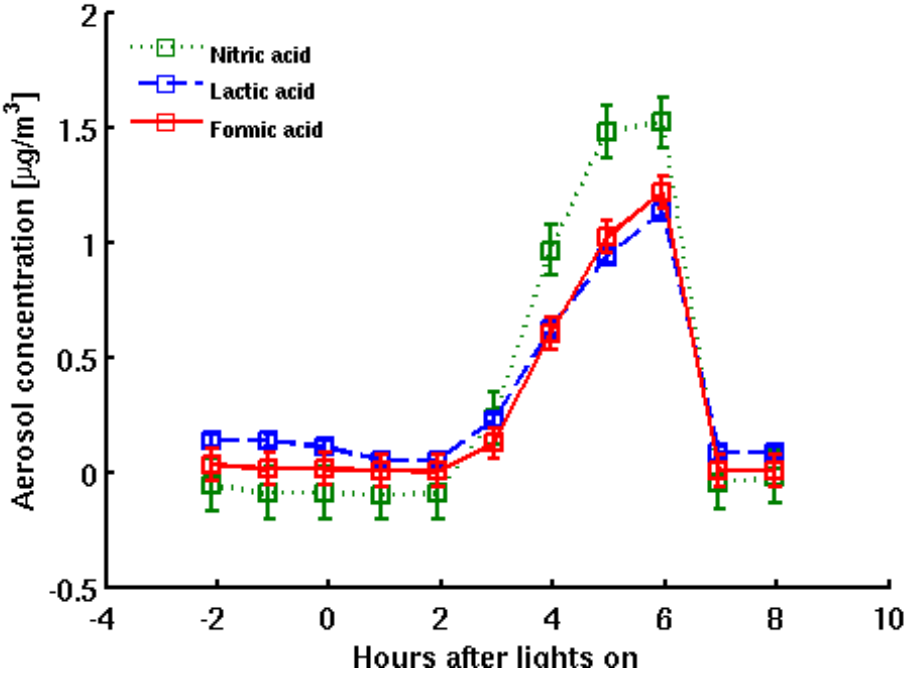

Fig. 1. No breakthrough of the gas phase to the aerosol collector (AC) was observed when a filter was placed 6 h after lights on in the aerosol sampling line during a 1200 ppbv 1,3,5-trimethylbenzene (TMB) photooxidation experiment.

ACPD
14, 985–1018, 2014

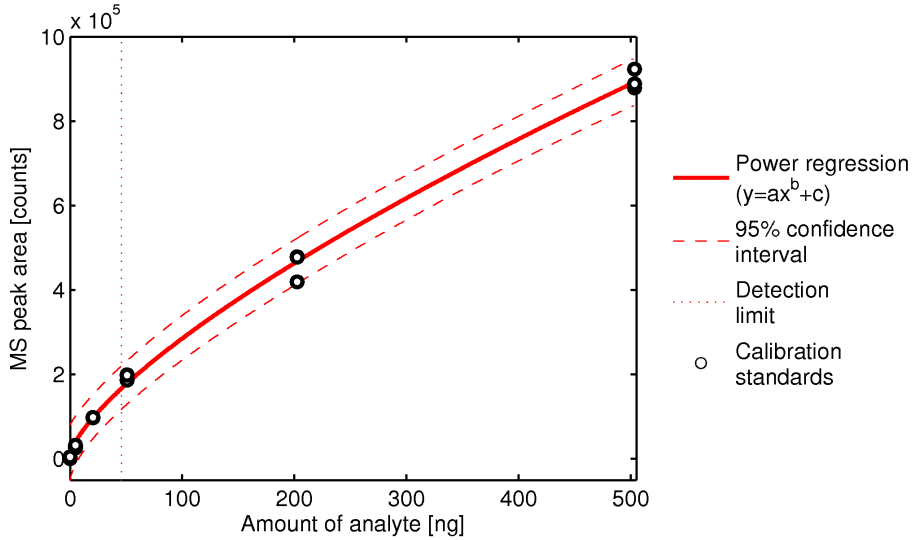

Fig. 2. Example of IC/MS calibration (methylmaleic acid).

ACPD
14, 985–1018, 2014

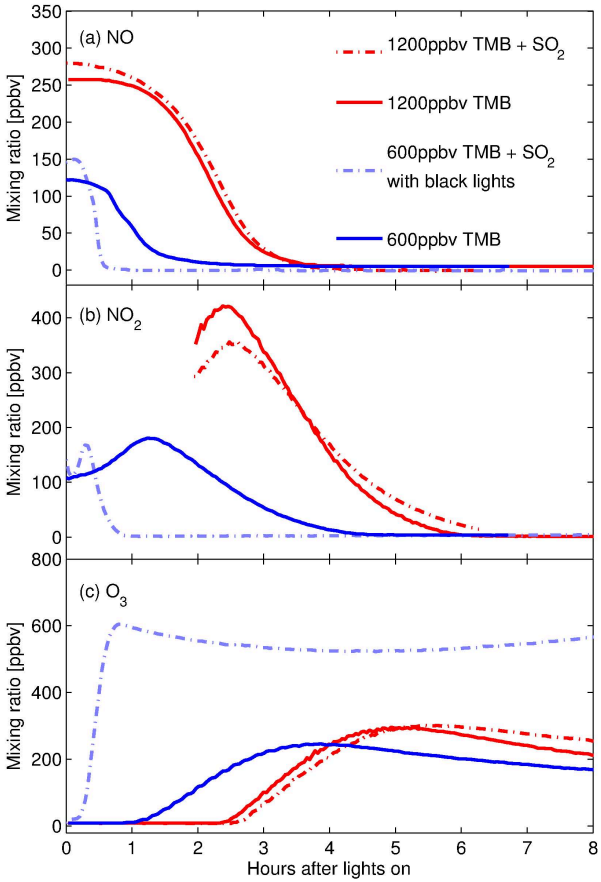

Fig. 3. Nitrogen oxide (NO, **a**), nitrogen dioxide (NO_2, **b**) and ozone (O_3, **c**) mixing ratios for the different experiments. High concentration experiments: red; low concentration experiments: blue; without SO_2: solid lines; with SO_2: dashed lines. NO_2 data is missing at the beginning of the high concentration experiments, due to an instrumental limitation.

ACPD
14, 985–1018, 2014

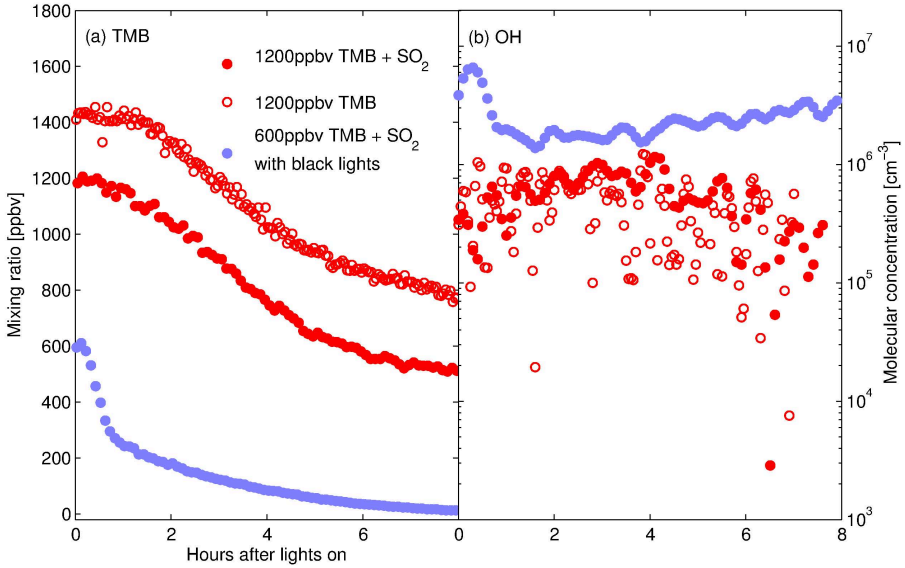

Fig. 4. 1,3,5-Trimethylbenzene (TMB, **a**) and derived hydroxyl radicals ($OH^{\bullet}$, **b**) concentrations for the different experiments. Filled symbols: with SO_2; open symbols: without SO_2; red: high conc.; blue: low conc.

ACPD
14, 985–1018, 2014

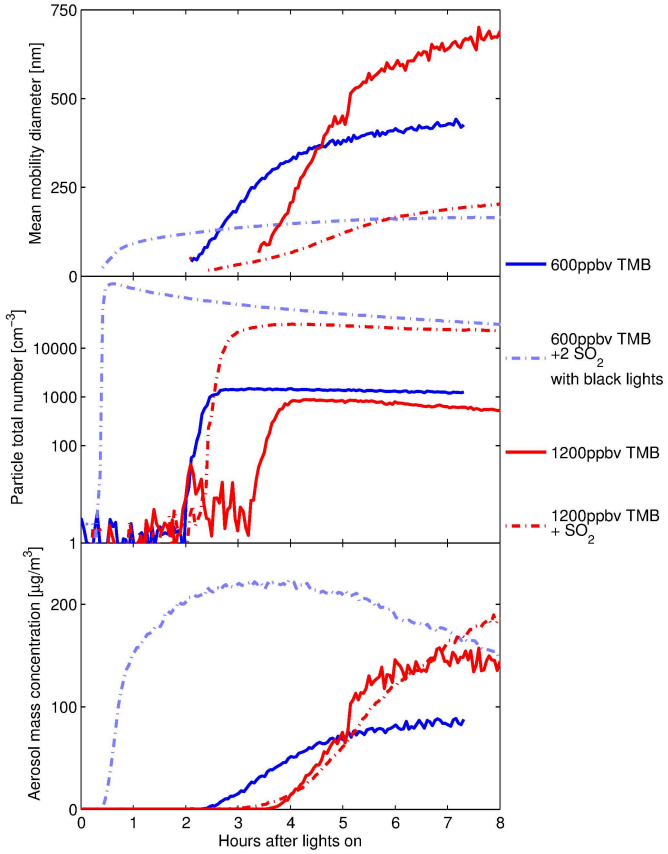

Fig. 5. Mean diameter, total number concentration and aerosol mass concentration (assuming $\rho = 1.4\,\mathrm{g\,cm^{-3}}$) from the scanning mobility particle sizer (SMPS) measurements. These data are not corrected for wall losses. High concentration experiments: red; low concentration experiments: blue; without SO_2: solid lines; with SO_2: dashed lines.

ACPD
14, 985–1018, 2014

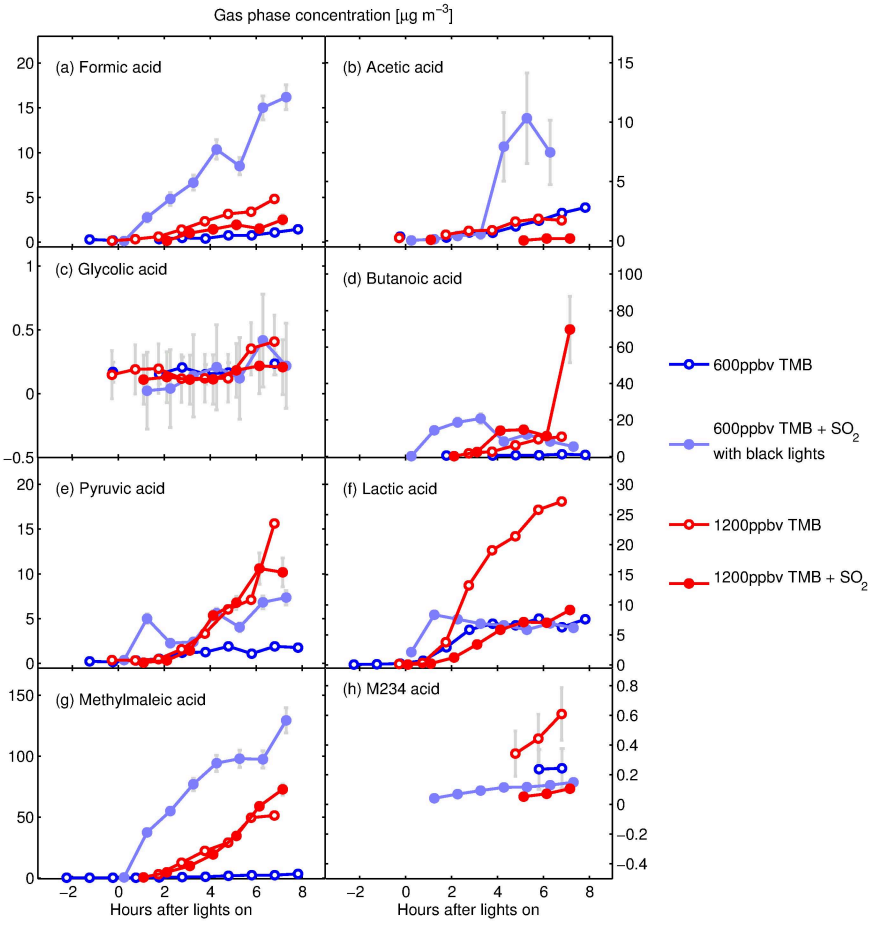

Fig. 6. Gas phase concentration profiles (in µg m^{-3}) of eight measured organic acids. Filled symbols: with SO_2; open symbols: without SO_2; red: high conc.; blue: low conc. Error bars in grey are derived from calibration curves and sampling flows uncertainties.

ACPD
14, 985–1018, 2014

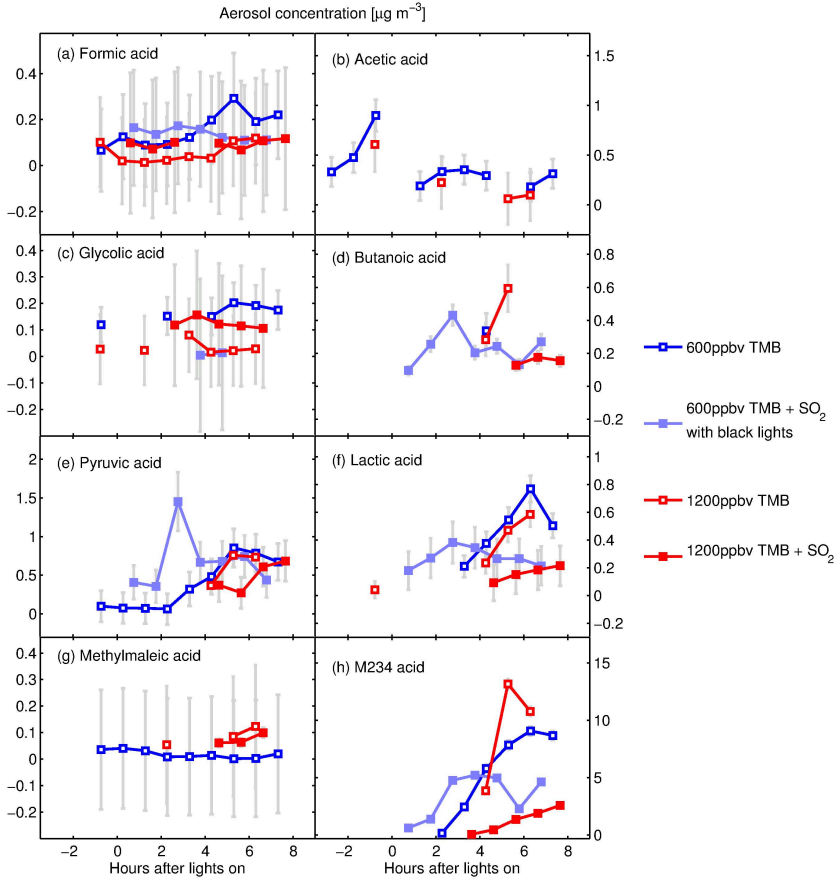

Fig. 7. Aerosol concentration profiles (in μg m^{-3}) of eight measured organic acids. See Fig. 6 for symbol explanation.

ACPD
14, 985–1018, 2014

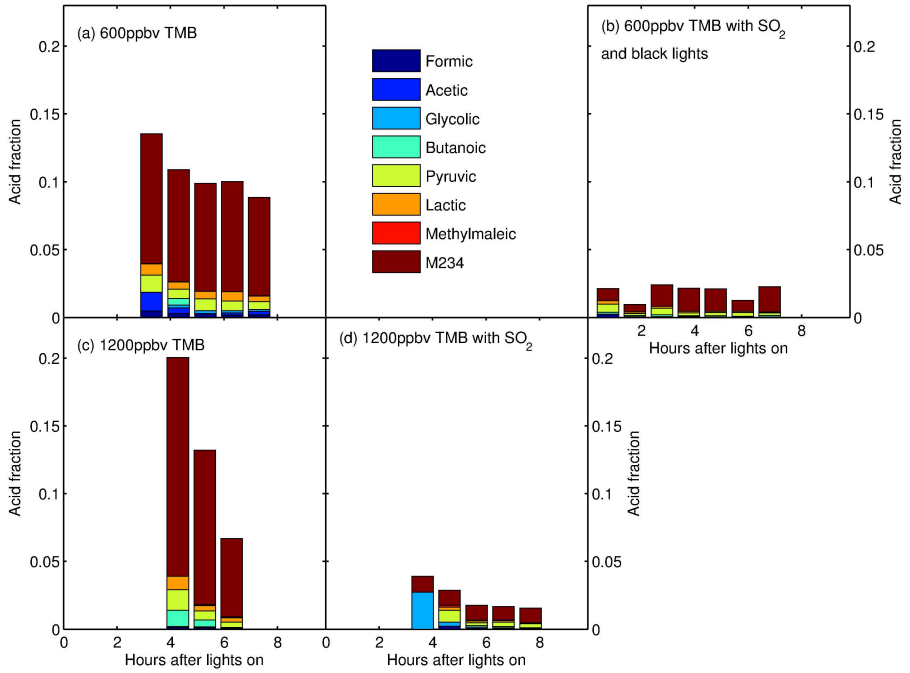

Fig. 8. Stacked normalized aerosol concentrations of the main detected organic acids for the different experimental conditions.

ACPD
14, 985–1018, 2014

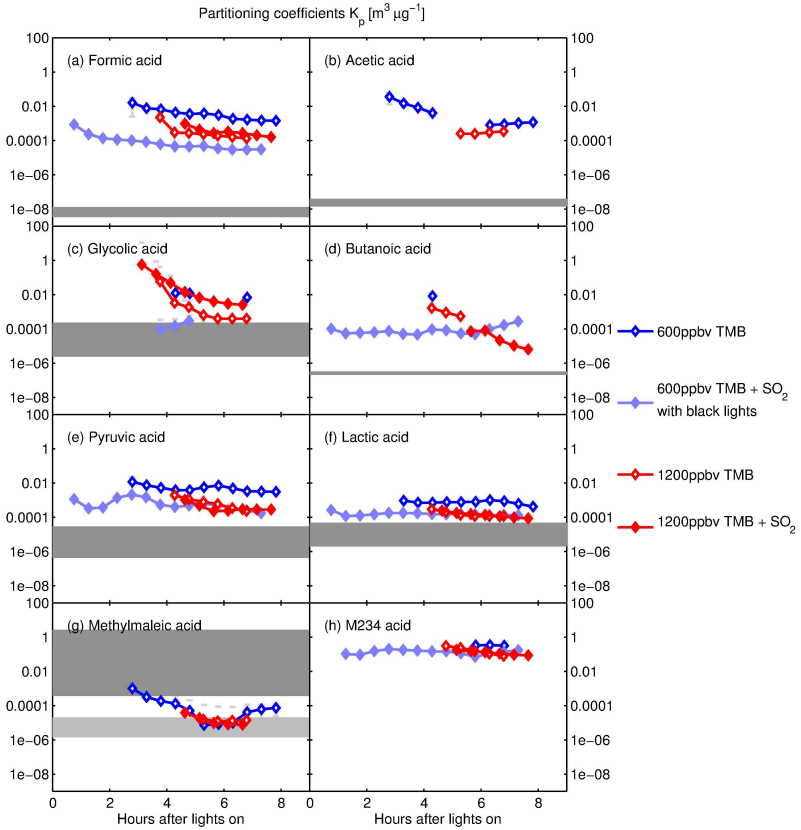

Fig. 9. Time-dependent partitioning coefficients, K_p (in $m^3\,\mu g^{-1}$). Grey areas represent the theoretical range values for different saturation vapour pressure estimations, where the upper limit assumes pH = 4 for the effective partitioning coefficient($K_{p,\,eff}$). See text for discussion. In **(g)**, the light grey area represents the theoretical range value of methylmaleic anhydride.

ACPD
14, 985–1018, 2014

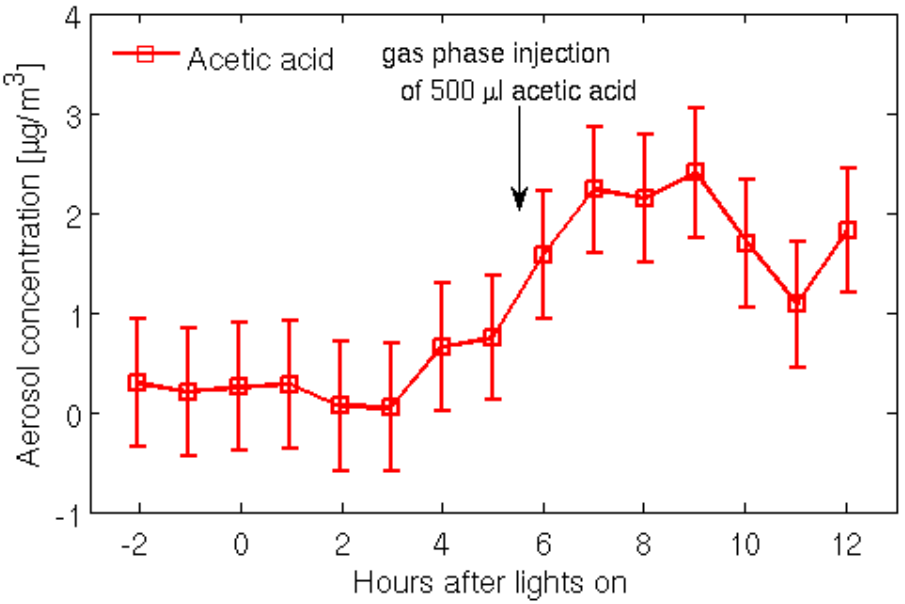

Fig. 10. No partitioning of acetic acid onto the aerosol is observed after injection of a large amount of acetic acid.

ACPD
14, 985–1018, 2014